ACS APPLIED MATERIALS & INTERFACES

www.acsami.org

Research Article

Boosting the Efficiency and Stability of Perovskite Light-Emitting Devices by a 3-Amino-1-propanol-Tailored PEDOT:PSS Hole Transport Layer

Ruiting Fan, Li Song,* Yongsheng Hu, Xiaoyang Guo, Xingyuan Liu,* Lishuang Wang, Chong Geng, Shu Xu, Yonghui Zhang, Zihui Zhang, Nannan Luan, and Wengang Bi*

Cite This: *ACS Appl. Mater. Interfaces* 2020, 12, 43331−43338

Read Online

ACCESS | Metrics & More | Article Recommendations | Supporting Information

ABSTRACT: Properties of the underlying hole transport layer (HTL) in perovskite light-emitting devices (PeLEDs) play a critical role in determining the optoelectronic performance through influencing both the charge transport and the quality of the active perovskite emission layer (EML). This work focuses on manipulating the carrier transport behavior and obtaining a high-quality EML film by tailoring the poly(3,4-ethylenedioxythiophene):poly(styrenesulfonate) (PEDOT:PSS) HTL with previously unused amino alcohol 3-amino-1-propanol (3AP). The modified PEDOT:PSS rendered a deeper work function that is more suitable for the hole injection from the HTL to EML. More importantly, the 3AP-modified PEDOT:PSS film can induce a low-dimensional perovskite phase that can passivate the defects in the EML, resulting in a significantly improved light emission. Such ameliorations consequently result in a dramatical enhancement in performance of PeLED with a low turn-on voltage of 2.54 V, a maximum luminance of 23033 cd/m^2, a highest current efficiency of 29.38 cd/A, a corresponding maximum external quantum efficiency of 9.4%, and a prolonged lifetime of 6.1 h at a proper Cs/Pb ratio.

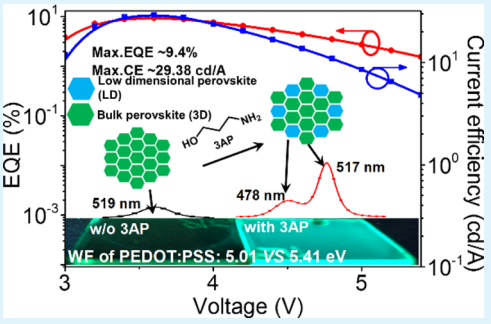

KEYWORDS: *perovskite light-emitting devices, 3-amino-1-propanol, modified PEDOT:PSS, $CsPbBr_3$, energy funneling*

INTRODUCTION

By virtue of the superior thermal and moisture stability,[1,2] all inorganic cesium lead halides ($CsPbX_3$, X = Cl, Br, and I) emerged as a novel material toward optoelectronics such as solar cells,[3,4] photodetector,[5] light-emitting devices (LED), and so on. The merits of high photoluminescence (PL) quantum efficiency,[6] high color purity, tunable wavelength,[7] and solution processability make them a competitive candidate in developing next-generation display technology.

Among efficient PeLEDs, poly(3,4-ethyl-enedioxythiophene):poly (styrenesulfonate) (PEDOT:PSS) is the widely employed hole transport layer (HTL) used to fabricate in situ $CsPbBr_3$ PeLEDs thanks to its low-temperature solution process;[8,9] whereas, there is an energy level difference of about 1.2 eV between the work function of PEDOT:PSS (~5.0 eV) and the deep HOMO level of $CsPbBr_3$ (~6.2 eV), which inhibits the effective injection of carriers and hinders the improvement of EL performance of perovskite PeLEDs. A widely adopted approach to improve the work function of PEDOT:PSS is introducing additives or inserting an interfacial layer and thereby reducing the energy barriers to facilitate the hole injection.[9−12] For instance, alcohols (e.g., methanol) are demonstrated to be effective additives to modify the work function of PEDOT:PSS.[9,13] It is worth mentioning that the chemical and physical properties of the underlying HTL would influence the morphology as well as the trap-mediated nonradiative loss of the overlying perovskite emission layer (EML). Hence, an efficient additive that can simultaneously reduce the energy barrier to ensure the efficient carrier transport and suppress the nonradiative recombination with high-quality morphology is highly desired.

It has been extensively demonstrated that nonradiative defect sites (such as unsaturated halide or Pb^{2+} vacancies) can be effectively passivated by implementing organic additives either into the perovskite precursors or as an interlayer through the interaction with their functional groups (e.g., $-NH_2$).[1,14−24] Among these efficient additives, large-group ammonium halides[21−24] (e.g., phenylethylammonium bromide, *n*-butylammonium bromide) can intercalate into the three-dimensional framework to form a low-dimensional (LD) perovskite, increase the exciton binding energy (E_b), and allow

Received: July 22, 2020
Accepted: August 25, 2020
Published: August 25, 2020

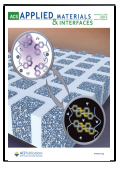

the occurrence of energy-funneling process among different layered perovskite phase and thereby achieve efficient radiative recombination. By this ingenious strategy, significant progress has been made to the efficient PeLED with external quantum efficiency (EQE) exceeding 10%.[24,25] Considering the above two aspects, the amino alcohols with both the −OH and the $-NH_2$ functional group may be suitable additives to assume a dual role in tuning the energy barrier and suppressing the nonradiative defects.

Herein, a new additive 3-amino-1-propanol (3AP) is utilized to modify the PEDOT:PSS. This strategy can significantly deepen the work function of PEDOT:PSS, which is conducive to the hole injection. More importantly, the 3AP-modified PEDOT:PSS can directly induce a LD/3D mixed perovskite EML, ensuring efficient radiative recombination without sacrificing the EML's conductivity. Such merits consequently resulted in significantly improved EL performance for the PeLEDs. By further exploring the influence of the Cs/Pb ratio in the precursor, an optimal PeLED with a maximum brightness of 23,033 cd/m^2, a maximum CE of 29.38 cd/A, a maximum EQE of ∼9.4%, and enhanced operational stability of ∼6.1 h was realized. Our results would provide a novel strategy to simultaneously deepen the work function of the PEDOT:PSS HTL and construct the efficient LD/3D perovskite EML via an energy funneling process toward achieving high-performance PeLEDs.

RESULTS AND DISCUSSION

As is known, the defects of the perovskite films are not only affected by stoichiometry and compositions of the precursors but also by the underlying interface.[16,26] We first investigate the properties of the 3AP-modified PEDOT:PSS and its influence on the overlying perovskite films. Figure 1a shows the molecular structure of the PEDOT:PSS and the employed 3AP. The addition of 3AP between the positively charged PEDOT chains and the negatively charged PSS chains would probably reduce their strong electrostatic coulombic interaction. Hence, the electrical conductivity of the PEDOT:PSS films that strongly depend on the film morphology and ratio between the highly conductive PEDOT and the poorly conductive PSS would be affected. The electrical characteristics of the PEDOT:PSS films were investigated by the hole-only devices (as shown in Figure S1a and depicted in Figure 1b). The linear $I-V$ characteristics confirms the high conductivity of both PEDOT:PSS films with and without 3AP. After the introduction of 3AP, the conductivity for the modified PEDOT:PSS film is marginally decreased. To make a deep insight of the conductivity reduction, atomic force microscopy (AFM) was adopted to investigate the 3AP influence on the PEDOT:PSS morphology. The AFM topography images in Figure 1d,e show that both PEDOT:PSS films without and with 3AP present a dense and smooth surface. The pristine PEDOT:PSS was composed of bigger particles and presented a higher root mean square (rms) roughness (∼2.29 nm) than that of the 3AP-modified films (rms ∼ 1.86 nm). The reduced particles and rms indicated that the incorporation of 3AP would not cause separation between PEDOT and PSS and lead to an inferior PEDOT crystallinity resulting in the decreased conductivity of the PEDOT:PSS. Figure S1b shows the X-ray photoelectron spectroscopy (XPS) results for the pristine PEDOT:PSS and the 3AP-modified PEDOT:PSS films. The higher binding energy peak at 167 eV is assigned to the sulfur signal of PSS, and the doublet signal at around 162−165 eV

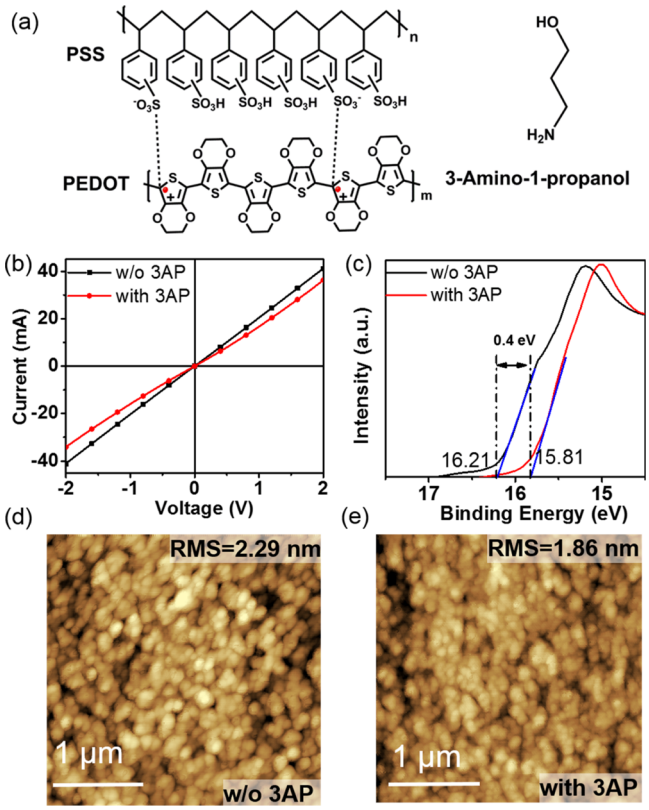

Figure 1. (a) Molecular structure of the PEDOT:PSS and 3AP molecules, (b) $I-V$ curves for the hole-only devices: ITO/PEDOT:PSS or 3AP-PEDOT:PSS/HAT-CN/Al, (c) high-binding energy secondary electron cutoff of the pristine and 3AP-modified PEDOT:PSS. AFM images for the (d) neat PEDOT:PSS film, and (e) 3AP-PEDOT:PSS film. The concentration of 3AP to tailor the PEDOT:PSS is 75 mg/mL in ethanol unless otherwise noted.

corresponds to the sulfur atoms in PEDOT. Evidently, the amount of PSS in the 3AP-modified PEDOT:PSS films is slightly increased compared with the pristine PEDOT:PSS films, which is responsible for the slightly reduced conductivity. More importantly, the energy level, a critical factor to regulate carrier transports, was surveyed by ultraviolet photoelectron spectroscopy (UPS), as shown in Figure 1c. The obtained work function for the neat PEDOT:PSS is 5.01 eV (by subtracting the secondary electron cutoff from the He 1α excitation energy 21.22 eV), which is in accordance with the previously reported values.[27,28] However, the secondary electron cutoff for the 3AP-modified PEDOT:PSS exhibits a redshift, leading to a work function of 5.41 eV. The deepened work function is desirable to facilitate hole transport from the HTL to $CsPbBr_3$ EML to achieve efficient PeLEDs.

The ratio variation between PEDOT and PSS would change the surface wettability and thereafter influence the growth of $CsPbBr_3$ perovskite EMLs. Contact angle measurements were utilized to investigate the surface properties of PEDOT:PSS films. As shown in Figure 2a,b, the DMSO precursors on the pristine PEDOT:PSS film exhibited a contact angle of 20.9°, whereas that on the 3AP-treated PEDOT:PSS film decreased to 12.3°. The better wetting property of the 3AP-treated PEDOT:PSS film can partially be attributed to the increased water-soluble PSS proportion. Because the boiling point of 3AP is as high as 184 °C, while the annealing temperature for the PEDOT:PSS films is 140 °C; hence, we speculate that the

https://dx.doi.org/10.1021/acsami.0c13214
ACS Appl. Mater. Interfaces 2020, 12, 43331−43338

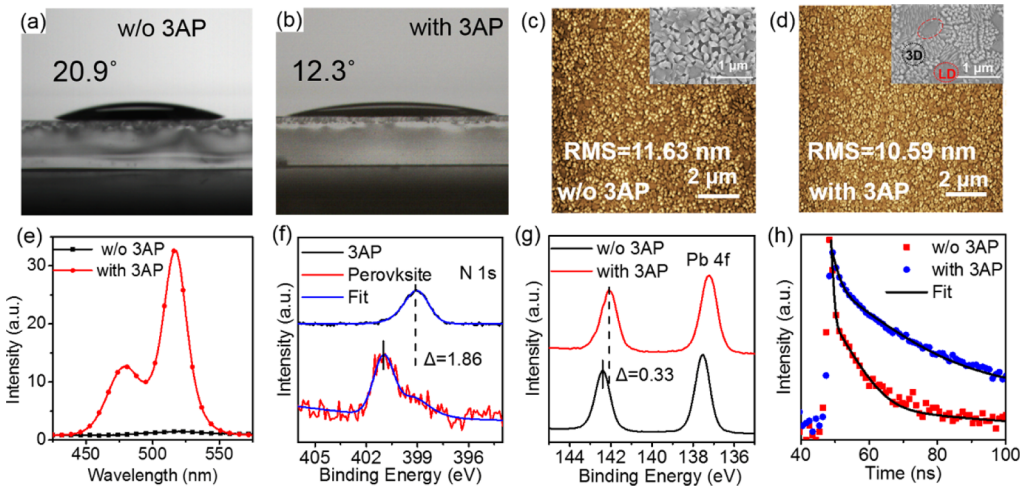

Figure 2. Contact angle of DMSO on (a) PEDOT:PSS and (b) 3AP-PEDOT:PSS films. AFM images of the $CsPbBr_3$ films deposited on (c) PEDOT:PSS and (d) 3AP-PEDOT:PSS films. (Insets are corresponding SEM images) (e) PL spectra of $CsPbBr_3$ films on neat PEDOT:PSS and 3AP-PEDOT:PSS films. XPS spectra of (f) N 1s for 3AP and perovskite on 3AP-PEDOT:PSS and (g) Pb 4f for the perovskite films on neat PEDOT:PSS and 3AP-PEDOT:PSS. (h) PL decay curves of $CsPbBr_3$ films on PEDOT:PSS and 3AP-PEDOT:PSS films monitored at their peak wavelength.

hydroxyl (−OH) functional group may also enhance the hydrophilicity of the PEDOT:PSS. To confirm our conjecture, we introduce propylamine, which has a similar $-NH_2$ functional group but lacks of −OH as compared with 3AP, into the PEDOT:PSS solutions and conducted the contact angle measurement (shown in Figure S2). The propylamine-modified PEDOT:PSS films exhibited a contact angle of 15.8° which is larger than the 3AP-treated PEDOT:PSS films, affirming that the remaining 3AP in the PEDOT:PSS film also contributes to better hydrophilicity. The ameliorated hydrophilicity would further influence the perovskite nucleation and consequently affect the morphology of the EML, as demonstrated in Figure 2c,d, where the EML on the pristine PEDOT:PSS is rougher (rms ∼ 11.63 nm) than that grown on the 3AP-modified PEDOT:PSS (rms ∼ 10.59 nm).

Next, we investigate the influence of the 3AP-PEDOT:PSS on the overlying $CsPbBr_3$ films when the Cs/Pb ratio is 1.86 in the precursors. Steady-state and TPRL measurements were employed to investigate the photophysical properties. As illustrated in Figure 2e, the $CsPbBr_3$ films directly formed on pristine PEDOT:PSS exhibit a weak intensity with a PL quantum yield (PLQY) <1% and a single peak at 519 nm, in line with the emission from bulk 3D $CsPbBr_3$,[29] while that for the EML formed on 3AP-modified PEDOT:PSS is dramatically enhanced with a PLQY of 36%. Accompanied by the enhancement of the PL emission, another peak with a higher energy at 478 nm appears, indicting the coexistence of two different perovskite phases in the films. Meanwhile, scanning electron microscopies (insets in Figure 2c,d) reveal that apart from the granular grains, which are similar to those of 3D films, some plate-like phases also emerged in the perovskite films formed on the 3AP-PEDOT:PSS. Correlating with the PL spectra, we deduce that the newly appeared grains (named LD perovskite) would be responsible for the shorter wavelength emission. We also use confocal laser scanning microscopy to investigate its light-emission properties from a microscopic perspective to confirm our speculation, as shown in Figure S3. Upon 405 nm excitation, the perovskite film on the 3AP-PEDOT:PSS presents green light-emitting dominated regions and sporadic blue light-emitting regions, reconfirming the coexistence of LD and 3D perovskite phases. It is worth noting that we did not observe the excitonic absorption signals corresponding to the higher band gap domains in the absorption spectra (Figure S4), which is probably enveloped by quasicontinuous absorptions as a previous work reported.[30] The appearance of the LD perovskite phase may be caused by the residual 3AP in the PEDOT:PSS, which would partially redissolve in the DMSO perovskite precursors during the spin-coating process and act as separation layers to impede the $CsPbBr_3$ crystal growth. X-ray diffraction patterns (Figure S5) demonstrate that the crystal structure of $CsPbBr_3$ is not affected by 3AP because no evident difference in the XRD diffraction peaks is observed except for the weakened diffraction intensity. To further confirm the interaction mechanism between 3AP and perovskite, XPS was employed to investigate the chemical states of the perovskite films. The high-resolution XPS spectrum of the perovskite film on 3AP-modified PEDOT:PSS presents a blueshifted N 1s signal at 399.09 eV compared with that in 3AP (N 1s 400.95 eV), verifying the existence of 3AP in the perovskite films. Meanwhile, the binding energy peak of Pb 4f has a slight redshift from 137.23 to 137.56 eV, indicating an increased electron shielding of the Pb atomic nucleus. The observations affirmed the important role of 3AP in forming the LD perovskite phase. It is worth noting that the energy transfer from the higher band gap domains to the lower band gap domains would occur inevitably in such multiphase coexistence films.[22,31] Such a process would increase the carrier density in the 3D domain and subsequently fill the available trap states, leading to the PL enhancement as was observed in our perovskite films. Although the additional peak may affect purity through broadening the spectra, they could also be beneficial in fine-tuning the energy landscape and regulating the behavior of the charge carriers, which would be of great importance to the EL performance. Time-resolved PL (TPRL) measurements also provide favorable evidence to disclose the energy transfer process. All the PL decay curves (Figure 2h) are well fitted by a tri-exponential decay function comprising fast defects or energy transfer-related nonradiative recombination τ_1, an intermediate component corresponding to the bimolecular

https://dx.doi.org/10.1021/acsami.0c13214
ACS Appl. Mater. Interfaces 2020, 12, 43331−43338

Table 1. Exciton Lifetimes of Perovskite Films Formed on PEDOT:PSS and 3AP-PEDOT:PSS Detected at the Corresponding Peak Wavelength

perovskite	peak (nm)	τ_1 (ns)	rel (%)	τ_2 (ns)	rel (%)	τ_3 (ns)	rel (%)	τ_{ave} (ns)
3D	519	0.36	85.63	4.03	11.73	56.17	3.00	2.47
LD/3D	517	1.41	22.79	11.83	50.09	55.69	27.12	21.35
	478	0.69	66.85	2.90	28.67	14.28	4.48	1.93

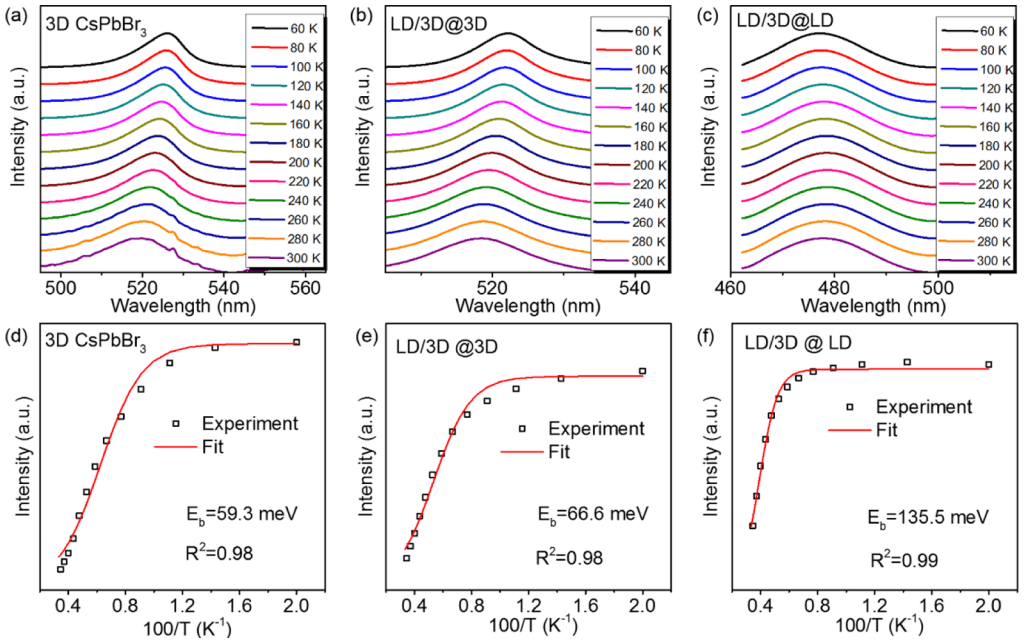

Figure 3. Temperature-dependent PL characteristics of 3D or LD/3D mixed perovskite films. (a–c) Normalized temperature-dependent PL spectra. (d–f) PL intensities at temperature of 60 to 300 K.

recombination of charge carriers τ_2 and a slowest component τ_3 relevant to the radiative recombination of free carriers. The parameters are tabulated in Table 1. For the perovskite on pristine PEDOT:PSS with a single phase, the nonradiative recombination accounts for a proportion of 85.63%, indicative of high defect density and responsible for the poor performance discussed below. In contrast, the emission at 517 nm in the perovskite film on 3AP-modified PEDOT:PSS exhibits a decreased proportion of nonradiative recombination (22.79%) and an increased proportion of free carriers, as listed in Table 1, suggesting more adequate carriers in the 3D domains in the multiphase perovskite films as compared with that in the pure 3D perovskite films. Moreover, the nonradiative recombination that probably originated from the energy transfer is also dominant in the LD perovskites. These observations reconfirm the energy funneling process in the perovskite film on 3AP-modified PEDOT:PSS.

The temperature-dependent PL spectrum was used to reveal the fundamental properties of the exciton in our perovskite films. Figure 3a–c displays the steady-state temperature-dependent PL spectra of the perovskites formed on pristine PEDOT:PSS (Figure 3a) and 3AP-modified PEDOT:PSS (Figure 3b for the bulk 3D emission in the mixed LD/3D perovskite and Figure 3c for the LD emission) excited by a 405 nm laser from 60 to 300 K with a step of 20 K. Overall, the luminescence peaks corresponding to the bulk $CsPbBr_3$ feature similar evolution tendencies (blueshifted PL peak and line width broadening) as the temperature increases. Generally, the peak shifts in the PL spectra can be originated from the joint influence of the thermal expansion effect of the lattice and exciton–phonon interactions. Typically, the former results in the band gap blueshift and the latter leads to the band gap redshift. Hence, in our cases, the thermal expansion effect rather than the exciton–phonon coupling dominates in the spectra evolution tendency for the bulk $CsPbBr_3$ perovskite. Such observations coincided well with previous reports;[18,32] whereas the luminescent peak synonymous with a band gap of 2.59 eV contrarily features a slightly gradual redshift from 478 to 479 nm, indicating that the exciton–phonon interactions overwhelming the thermal expansion effects. The suppression of thermal expansion in the LD perovskites can be ascribed to the compression effect which originated from the bulky organic moisture which has been also observed in many other LD perovskites.[33,34] In addition, the PL intensity is more dependent on the temperature, as shown in Figure 3d–f. The exciton binding energy (E_b), which affects the exciton dissociation probability, can be extracted from the PL intensity-temperature relationship by the following equation

$$I(T) = \frac{I_0}{1 + A\, e^{-E_b/k_B T}} \quad (1)$$

where I_0 and k_B are the PL intensity at 0 K and Boltzmann's constant, respectively. For the bulk $CsPbBr_3$ phase, both on PEDOT:PSS and 3AP-PEDOT:PSS, the fitted E_b values are 59.3 and 66.6 meV, respectively, which agree well with those in previous reports.[29] The E_b is enlarged to 135.5 meV for the LD perovskite phase owing to the quantum and dielectric confinement, facilitating the exciton formation and suppressing the exciton dissociation. Such observations would result in enhanced light emission coinciding well with the PL results.

https://dx.doi.org/10.1021/acsami.0c13214
ACS Appl. Mater. Interfaces 2020, 12, 43331–43338

Encouraged by the enhancement of the PL emission and the energy level tuning ability which would be beneficial to promote the EL performance, we further examined the potential of the modified PEDOT:PSS in fabricating efficient PeLED. We first scrutinized the influence of the doping concentration of 3AP in PEDOT:PSS to obtain the optimal EL performance using a fixed CsBr:$PbBr_2$ molar ratio of 1.86. Figure 4a displays that the device structure employed in this

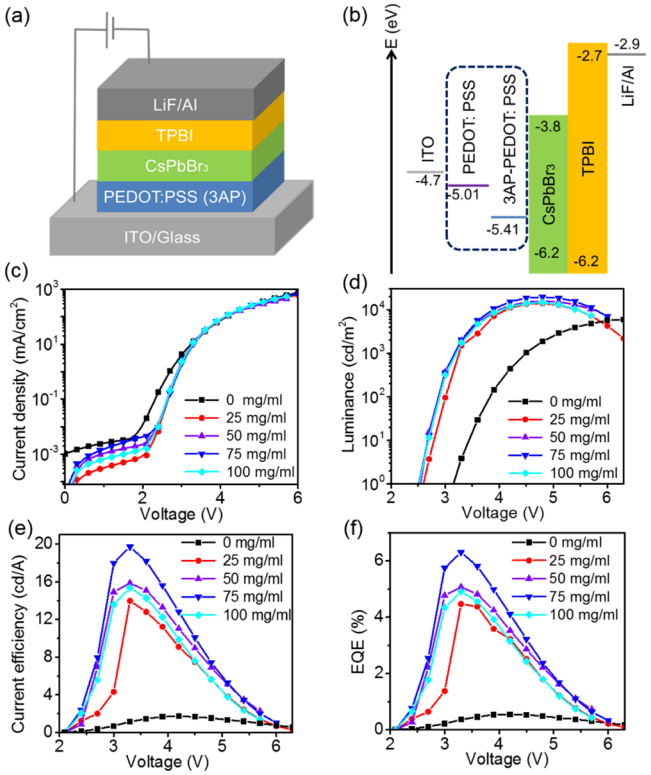

Figure 4. (a) Device structure of the PeLED. (b) Energy diagram of each layer for the PeLED device. (c) Current density, (d) luminance, (e) current efficiency, and (f) EQE as a function of driving voltage for the PeLEDs with different concentrations of 3AP-modified PEDOT:PSS films.

work and the corresponding energy level diagram for all the functional layers is given in Figure 4b. The 3AP was first dissolved in ethanol with different weight ratios (0, 25, 50, 75, and 100 mg/mL) and then mixed with a PEDOT:PSS solution at a volume ratio of 1:10. For simplicity and differentiation, we defined the device with the 3AP doping amount. Figure 4c–f shows the J–V (current density vs voltage), L–V (luminance vs voltage), CE–V (current efficiency vs voltage), and EQE–V relationships. All the devices show negligible leakage current. The control device with pristine PEDOT:PSS as the HTL shows a relatively poor optoelectronic performance with a turn-on voltage of 3.15 V and achieves a maximum brightness of 5990 cd/m^2, a highest CE of 1.73 cd/A and a corresponding EQE of 0.54% (also see detailed parameters summarized in Table S1). Remarkably, the turn-on voltage is dramatically reduced from 3.15 V for the PeLED with pristine PEDOT:PSS HTL to around 2.51 V for that with the 3AP-modified PEDOT:PSS HTL (75 mg/mL). The decrease in turn-on voltage can be ascribed to the decreased energy barrier between the work function of the 3AP-modified PEDOT:PSS and the valance band of $CsPbBr_3$ (see Figure 1c), enabling sufficient injection of the hole carriers into EML. Meanwhile, the PeLEDs with 3AP-modified PEDOT:PSS exhibit a gradual increase both in maximum luminance and efficiency as the 3AP doping ratio gradually increases and achieved the highest brightness of 19,558 cd/m^2, highest CE of 19.71 cd/A, and the highest EQE of 6.31% at a 3AP weight ratio of 75 mg/mL. The promotion in EL performance is likely due to an accumulation of several benefits caused by 3AP: (a) the mobility of PEDOT:PSS (4.5×10^{-2} cm^2 V^{-1} s^{-1})[35] is much higher than that of TPBI (3.3×10^{-5} cm^2 V^{-1} s^{-1}),[36] resulting in the unbalance in charge transport. The introduction of 3AP into PEDOT:PSS could slightly decrease the conductivity of the HTL, which is beneficial to regulate the charge transport balance. (b) The 3AP-modified PEDOT:PSS has a more suitable work function in favor of hole injection into the $CsPbBr_3$ EML, alleviating carrier accumulation at the HTL/EML interface. (c) The induced LD perovskite phase could enhance the light-emission by energy funneling.[37] A further increase in the 3AP weight ratio results in a reduction of the performance, which is probably due to the overregulation of charge balance.

Keeping in mind that stoichiometry of the precursors may play a crucial role in determining the EL performance, we further investigated the influence of the Cs/Pb ratio aiming at realizing better overall EL performance. The characteristic for the PeLEDs with different Cs/Pb ratios adopting 3AP (75 mg/mL)-modified PEDOT:PSS as the HTL is plotted in Figure 5 and related parameters are summarized in Table 2. When the Cs/Pb ratio is 1.71, the PeLED presents the best overall performance with a L_{max} of 23,033 cd/m^2, CE_{max} of 29.38 cd/A, and corresponding maximum EQE of 9.4%. Such performances are comparable to those reported efficient Cs-based PeLEDs, which also adopted the modified PEDOT:PSS (see Table S2). Although there exist two peaks in the PL spectra (Figure 2e), the device shows a narrow line-shaped spectra with a FWHM of 18 nm under the electrical-driven conditions below 5 V, before which the maximum CE and brightness have already been achieved, rendering high color purity CIE coordinates of (0.09, 0.61). The almost disappeared peak at 478 nm suggests the complete energy transfer from the larger band gap LD perovskite donors to the smaller band gap $CsPbBr_3$ bulk perovskite. The difference between EL and PL spectra could be owing to the different excitonic state formation mechanisms. Upon optical excitation, the excitons can be directly generated at a higher excitonic state, enabling the emission from both the LD and 3D perovskite phases, whereas, under electrical-driven conditions, the carriers might be trapped by the low band gap component, resulting in the emission from the 3D phase being dominant in the EL spectra. Concomitantly, we also found that the operation stability for the PeLED with 3AP-modified PEDOT:PSS as the HTL was dramatically prolonged with a lifetime of 6.1 h in contrast to the control device, which has a lifetime of merely 0.3 h, highlighting the important contribution made by 3AP in passivating the deleterious defects in the perovskites. Such inferior working stability may originate from the simple encapsulation used in our study, which is insufficient to fully isolate the PeLEDs from water, resulting in the degradation when operated in air for a longer time. Apart from this, the defects existed in the perovskites may accelerate the ion migration, which is considered to be responsible for the poor working stability. There would be much more improvements

https://dx.doi.org/10.1021/acsami.0c13214
ACS Appl. Mater. Interfaces 2020, 12, 43331−43338

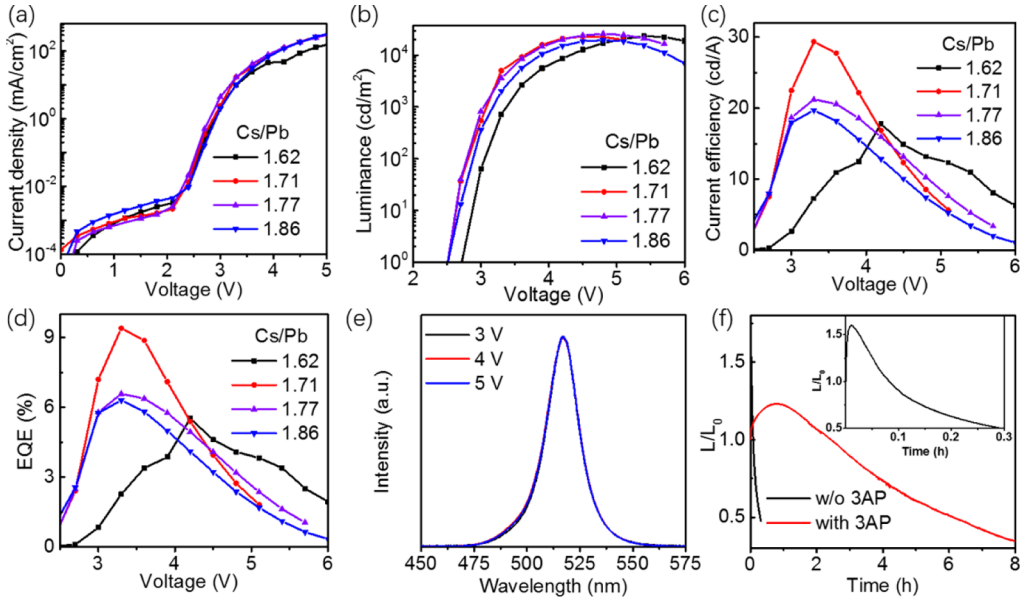

Figure 5. (a) $J-V$ curves, (b) $L-V$ curves, (c) CE$-V$ curves, and (d) EQE$-V$ curves of the PeLEDs with different Cs/Pb molar ratios. (e) EL spectra of the PeLEDs at different voltages. (f) Lifetime of the PeLEDs with PEDOT:PSS and 3AP-modified PEDOT:PSS at an initial luminance of 100 cd/m^2.

Table 2. EL Performance of the PeLED with Different Cs/Pb Molar Ratios When the 3AP Weight Ratio is 75 mg/mL

Cs/Pb molar ratio	max luminance (cd/m^2)	max CE (cd/A)	max EQE (%)	V_{on} (V)
1.62	23,385	17.81	5.52	2.72
1.71	23,033	29.38	9.40	2.54
1.77	25,855	21.24	6.58	2.51
1.86	19,558	19.71	6.31	2.51

for both the EL performance and stability of the PeLEDs if the bulk or the interfacial defects can be significantly suppressed.

CONCLUSIONS

In summary, efficient $CsPbBr_3$ PeLEDs have been realized by modifying the PEDOT:PSS HTL with 3AP molecules. The 3AP can help to form a smoother perovskite film by enhancing the DMSO's affinity, regulate the carrier transport by reducing the conductivity, and deepen the work function of the HTL simultaneously. Moreover, the radiative recombination via energy transfer is also promoted by inducing the mixed LD/3D perovskite phase. As a result, a better overall EL performance with a brightness of 23,033 cd/m^2, a CE of 29.38 cd/A, an EQE of 9.4%, and an enhanced working stability of 6.1 h have been achieved. This work would provide beneficial suggestions for the development of efficient PeLEDs.

EXPERIMENTAL SECTION

Materials. PEDOT:PSS (poly(3,4-ethylenedioxythiophene):poly(styreneulfonate)), lead(II) bromide ($PbBr_2$) (99.9%), and TPBi (1,3,5-tris (2-*N*-phenylbenzimidazolyl)-benzene) were purchased from Xi'an Polymer Light Technology Corp. Cesium bromide (CsBr) (99.9%) was purchased from Kanto Chemical Co., Inc. 3AP was purchased from Aladdin. All materials were used as received without further purification.

Film Fabrication and Characterization. The 3AP was first dissolved in ethanol to form a solution with different concentrations (25, 50, 75, and 100 mg/mL) and then the prepared 3AP solutions were mixed with PEDOT:PSS in a volume ratio of 1:10 and stirred uniformly. CsBr (45 mg) and 42 mg of $PbBr_2$ (molar ratio of 1.86) was mixed in 0.6 mL of the DMSO solvent and stirred overnight at 50 °C to form a transparent perovskite precursor. For other Cs/Pb molar ratios, the perovskite precursor was formed at a fixed weight concentration of 145 mg/mL. AFM (Shimadzu SPA-9700) was measured to characterize the morphology of the PEDOT:PSS or perovskite films. The PL spectra were acquired by using a Hitachi fluorescence spectrometer F-7000. The transient PL decay properties were measured with an Edinburgh FLS920 spectrometer. Absorption spectra of the perovskite film were measured using a Shimadzu UV-3101 PC spectrophotometer. XPS spectra were acquired by Escalab 250Xi. Temperature-dependent PL spectra were carried out using a Horiba iHR550 system equipped with 405 nm solid-state lasers and a helium-follow cryostat with temperatures from 60 to 300 K. The contact angles of DMSO on PEDOT:PSS and 3AP-PEDOT:PSS substrates were obtained by a contact angle analyzer JD2000. UPS spectra were carried out using an ESCALAB 250Xi with a monochromatized HeI (21.22 eV) excitation source. Confocal laser scanning microscopy was performed using a Nikon Eclipse Ti2 microscope. The XRD patterns of perovskite films were measured by Rigaku SmartLab.

Device Fabrication and Characterization. Prior to the device fabrication, ITO substrates were cleaned with deionized water, ethanol, and acetone solvents in sequence, and then treated with UV–ozone for 20 min. Then, the PEDOT:PSS with different concentrations of 3AP was spin-coated on the ITO substrates at 2500 rpm for 45 s and baked at 140° for 20 min on a hot plate under ambient air. After that, the perovskite solution was spin-coated at 5000 rpm for 60 s and annealed at 70° for 10 min in the N_2 filled glovebox. Subsequently, TPBi (40 nm), LiF (2 nm), and Al (100 nm) were successively thermally evaporated in a vacuum chamber (QHV-R20) under a pressure of below 4×10^{-4} Pa. The active area of the PeLED is 0.08 cm^2. The PeLED's luminance and current density were measured using a Keithley 2400 source meter and a luminance meter LS160. The EL spectra were recorded by an AvaSpec-ULS2048L fiber spectrometer. EQE was calculated from the brightness, current, and EL spectrum. All measurements were performed in air with encapsulation.

https://dx.doi.org/10.1021/acsami.0c13214
ACS Appl. Mater. Interfaces 2020, 12, 43331−43338

■ ASSOCIATED CONTENT

Supporting Information

The Supporting Information is available free of charge at https://pubs.acs.org/doi/10.1021/acsami.0c13214.

Device structure of the hole-only device, XPS spectra, confocal PL images, XRD spectra, and absorption curves (PDF)

■ AUTHOR INFORMATION

Corresponding Authors

Li Song − *State Key Laboratory of Reliability and Intelligence of Electrical Equipment and Tianjin Key Laboratory of Electronic Materials and Devices, School of Electronics and Information Engineering, Hebei University of Technology, Tianjin 300401, P. R. China;* orcid.org/0000-0002-4781-4023; Email: songli@hebut.edu.cn

Xingyuan Liu − *State Key Laboratory of Luminescence and Applications, Changchun Institute of Optics, Fine Mechanics and Physics, Chinese Academy of Sciences, Changchun 130033, China;* orcid.org/0000-0002-9681-1646; Email: liuxy@ciomp.ac.cn

Wengang Bi − *State Key Laboratory of Reliability and Intelligence of Electrical Equipment and Tianjin Key Laboratory of Electronic Materials and Devices, School of Electronics and Information Engineering, Hebei University of Technology, Tianjin 300401, P. R. China;* orcid.org/0000-0001-7736-8450; Email: wbi@hebut.edu.cn

Authors

Ruiting Fan − *State Key Laboratory of Reliability and Intelligence of Electrical Equipment and Tianjin Key Laboratory of Electronic Materials and Devices, School of Electronics and Information Engineering, Hebei University of Technology, Tianjin 300401, P. R. China*

Yongsheng Hu − *State Key Laboratory of Luminescence and Applications, Changchun Institute of Optics, Fine Mechanics and Physics, Chinese Academy of Sciences, Changchun 130033, China;* orcid.org/0000-0002-8116-4378

Xiaoyang Guo − *State Key Laboratory of Luminescence and Applications, Changchun Institute of Optics, Fine Mechanics and Physics, Chinese Academy of Sciences, Changchun 130033, China;* orcid.org/0000-0003-0259-137X

Lishuang Wang − *College of Chemistry and Chemical Engineering and Nano and Energy Research Center, School of Physics Science and Technology; Key Lab of Featured Metal Resources Utilization and Advanced Materials Development, Guangxi University, Nanning 530004, China;* orcid.org/0000-0003-0258-2481

Chong Geng − *State Key Laboratory of Reliability and Intelligence of Electrical Equipment and Tianjin Key Laboratory of Electronic Materials and Devices, School of Electronics and Information Engineering, Hebei University of Technology, Tianjin 300401, P. R. China*

Shu Xu − *State Key Laboratory of Reliability and Intelligence of Electrical Equipment and Tianjin Key Laboratory of Electronic Materials and Devices, School of Electronics and Information Engineering, Hebei University of Technology, Tianjin 300401, P. R. China;* orcid.org/0000-0002-4185-1392

Yonghui Zhang − *State Key Laboratory of Reliability and Intelligence of Electrical Equipment and Tianjin Key Laboratory of Electronic Materials and Devices, School of Electronics and Information Engineering, Hebei University of Technology, Tianjin 300401, P. R. China*

Zihui Zhang − *State Key Laboratory of Reliability and Intelligence of Electrical Equipment and Tianjin Key Laboratory of Electronic Materials and Devices, School of Electronics and Information Engineering, Hebei University of Technology, Tianjin 300401, P. R. China;* orcid.org/0000-0003-0638-1118

Nannan Luan − *State Key Laboratory of Reliability and Intelligence of Electrical Equipment and Tianjin Key Laboratory of Electronic Materials and Devices, School of Electronics and Information Engineering, Hebei University of Technology, Tianjin 300401, P. R. China*

Complete contact information is available at: https://pubs.acs.org/10.1021/acsami.0c13214

Notes

The authors declare no competing financial interest.

■ ACKNOWLEDGMENTS

The authors wish to thank Dr Wei Wang for his assistance with contact angle measurement. This work is supported by the Natural Science Foundation of Hebei Province (nos. F2019202252, F2019202294), the State Key Laboratory of Luminescence and Applications (no. SKLA-2019-07), the National Natural Science Foundation of China (nos. 61774154, 51672068, 51902082), the Jilin Province Science and Technology Research Project (no. 20180201029GX), Natural Science Foundation of Tianjin (no. 17JCYBJC41500), the Project funded by China Postdoctoral Science Foundation (no. 2019M653808XB), and the 2018 Guangxi Post-Doctoral Innovative Talent Support Program.

■ REFERENCES

(1) Ling, Y.; Tian, Y.; Wang, X.; Wang, J. C.; Knox, J. M.; Perez-Orive, F.; Du, Y.; Tan, L.; Hanson, K.; Ma, B.; Gao, H. Enhanced Optical and Electrical Properties of Polymer-Assisted All-Inorganic Perovskites for Light-Emitting Diodes. *Adv. Mater.* **2016**, *28*, 8983−8989.

(2) Shan, Q.; Li, J.; Song, J.; Zou, Y.; Xu, L.; Xue, J.; Dong, Y.; Huo, C.; Chen, J.; Han, B.; Zeng, H. All-Inorganic Quantum-Dot Light-Emitting Diodes Based on Perovskite Emitters with Low Turn-on Voltage and High Humidity Stability. *J. Mater. Chem. C* **2017**, *5*, 4565−4570.

(3) Beal, R. E.; Slotcavage, D. J.; Leijtens, T.; Bowring, A. R.; Belisle, R. A.; Nguyen, W. H.; Burkhard, G. F.; Hoke, E. T.; McGehee, M. D. Cesium Lead Halide Perovskites with Improved Stability for Tandem Solar Cells. *J. Phys. Chem. Lett.* **2016**, *7*, 746−751.

(4) Lau, C. F. J.; Zhang, M.; Deng, X.; Zheng, J.; Bing, J.; Ma, Q.; Kim, J.; Hu, L.; Green, M. A.; Huang, S.; Ho-Baillie, A. Strontium-Doped Low-Temperature-Processed CsPbI2Br Perovskite Solar Cells. *ACS Energy Lett.* **2017**, *2*, 2319−2325.

(5) Kang, C. H.; Dursun, I.; Liu, G.; Sinatra, L.; Sun, X.; Kong, M.; Pan, J.; Maity, P.; Ooi, E.-N.; Ng, T. K.; Mohammed, O. F.; Bakr, O. M.; Ooi, B. S. High-Speed Colour-Converting Photodetector with All-Inorganic $CsPbBr_3$ Perovskite Nanocrystals for Ultraviolet Light Communication. *Light: Sci. Appl.* **2019**, *8*, 94.

(6) Swarnkar, A.; Chulliyil, R.; Ravi, V. K.; Irfanullah, M.; Chowdhury, A.; Nag, A. Colloidal CsPbBr3Perovskite Nanocrystals: Luminescence beyond Traditional Quantum Dots. *Angew. Chem., Int. Ed.* **2015**, *54*, 15424−15428.

(7) Protesescu, L.; Yakunin, S.; Bodnarchuk, M. I.; Krieg, F.; Caputo, R.; Hendon, C. H.; Yang, R. X.; Walsh, A.; Kovalenko, M. V. Nanocrystals of Cesium Lead Halide Perovskites (CsPbX3, X = Cl,

Br, and I): Novel Optoelectronic Materials Showing Bright Emission with Wide Color Gamut. *Nano Lett.* **2015**, *15*, 3692−3696.
(8) Lee, B. R.; Yu, J. C.; Park, J. H.; Lee, S.; Mai, C.-K.; Zhao, B.; Wong, M. S.; Jung, E. D.; Nam, Y. S.; Park, S. Y.; Di Nuzzo, D.; Kim, J. Y.; Stranks, S. D.; Bazan, G. C.; Choi, H.; Song, M. H.; Friend, R. H. Conjugated Polyelectrolytes as Efficient Hole Transport Layers in Perovskite Light-Emitting Diodes. *ACS Nano* **2018**, *12*, 5826−5833.
(9) Wang, Z.; Li, Z.; Zhou, D.; Yu, J. Low Turn-on Voltage Perovskite Light-Emitting Diodes with Methanol Treated PEDOT:PSS as Hole Transport Layer. *Appl. Phys. Lett.* **2017**, *111*, 233304.
(10) Kim, D. B.; Yu, J. C.; Nam, Y. S.; Kim, D. W.; Jung, E. D.; Lee, S. Y.; Lee, S.; Park, J. H.; Lee, A.-Y.; Lee, B. R.; Di Nuzzo, D.; Friend, R. H.; Song, M. H. Improved performance of perovskite light-emitting diodes using a PEDOT:PSS and MoO3 composite layer. *J. Mater. Chem. C* **2016**, *4*, 8161−8165.
(11) Kim, Y.-H.; Cho, H.; Heo, J. H.; Kim, T.-S.; Myoung, N.; Lee, C.-L.; Im, S. H.; Lee, T.-W. Multicolored Organic/Inorganic Hybrid Perovskite Light-Emitting Diodes. *Adv. Mater.* **2015**, *27*, 1248−1254.
(12) Peng, X.-F.; Wu, X.-Y.; Ji, X.-X.; Ren, J.; Wang, Q.; Li, G.-Q.; Yang, X.-H. Modified Conducting Polymer Hole Injection Layer for High-Efficiency Perovskite Light-Emitting Devices: Enhanced Hole Injection and Reduced Luminescence Quenching. *J. Phys. Chem. Lett.* **2017**, *8*, 4691−4697.
(13) Wu, M.; Zhao, D.; Wang, Z.; Yu, J. High-Luminance Perovskite Light-Emitting Diodes with High-Polarity Alcohol Solvent Treating PEDOT:PSS as Hole Transport Layer. *Nanoscale Res. Lett.* **2018**, *13*, 128.
(14) Lee, S.; Park, J. H.; Lee, B. R.; Jung, E. D.; Yu, J. C.; Di Nuzzo, D.; Friend, R. H.; Song, M. H. Amine-Based Passivating Materials for Enhanced Optical Properties and Performance of Organic-Inorganic Perovskites in Light-Emitting Diodes. *J. Phys. Chem. Lett.* **2017**, *8*, 1784−1792.
(15) deQuilettes, D. W.; Koch, S.; Burke, S.; Paranji, R. K.; Shropshire, A. J.; Ziffer, M. E.; Ginger, D. S. Photoluminescence Lifetimes Exceeding 8 μs and Quantum Yields Exceeding 30% in Hybrid Perovskite Thin Films by Ligand Passivation. *ACS Energy Lett.* **2016**, *1*, 438−444.
(16) Song, L.; Guo, X.; Hu, Y.; Lv, Y.; Lin, J.; Liu, Z.; Fan, Y.; Liu, X. Efficient Inorganic Perovskite Light-Emitting Diodes with Polyethylene Glycol Passivated Ultrathin CsPbBr3 Films. *J. Phys. Chem. Lett.* **2017**, *8*, 4148−4154.
(17) Liu, X.; Guo, X.; Lv, Y.; Hu, Y.; Fan, Y.; Lin, J.; Liu, X.; Liu, X. High Brightness and Enhanced Stability of CsPbBr 3 -Based Perovskite Light-Emitting Diodes by Morphology and Interface Engineering. *Adv. Opt. Mater.* **2018**, *6*, 1801245.
(18) Song, L.; Guo, X.; Hu, Y.; Lv, Y.; Lin, J.; Fan, Y.; Zhang, N.; Liu, X. Improved performance of CsPbBr3 perovskite light-emitting devices by both boundary and interface defects passivation. *Nanoscale* **2018**, *10*, 18315−18322.
(19) Sun, S.-Q.; Hua, X.-C.; Liu, Q.-W.; Wang, T.-T.; Luo, W.; Zhang, Y.-J.; Liao, L.-S.; Fung, M.-K. Influence of a Lecithin Additive on the Performance of All-Inorganic Perovskite Light-Emitting Diodes. *J. Mater. Chem. C* **2019**, *7*, 2905−2910.
(20) Wang, K.-H.; Peng, Y.; Ge, J.; Jiang, S.; Zhu, B.-S.; Yao, J.; Yin, Y.-C.; Yang, J.-N.; Zhang, Q.; Yao, H.-B. Efficient and Color-Tunable Quasi-2D CsPbBrxCl3-x Perovskite Blue Light-Emitting Diodes. *ACS Photonics* **2019**, *6*, 667−676.
(21) Wang, Z.; Wang, F.; Sun, W.; Ni, R.; Hu, S.; Liu, J.; Zhang, B.; Alsaed, A.; Hayat, T.; Tan, Z. a. Manipulating the Trade-Off between Quantum Yield and Electrical Conductivity for High-Brightness Quasi-2D Perovskite Light-Emitting Diodes. *Adv. Funct. Mater.* **2018**, *28*, 1804187.
(22) Chen, P.; Meng, Y.; Ahmadi, M.; Peng, Q.; Gao, C.; Xu, L.; Shao, M.; Xiong, Z.; Hu, B. Charge-Transfer Versus Energy-Transfer in Quasi-2D Perovskite Light-Emitting Diodes. *Nano Energy* **2018**, *50*, 615−622.
(23) Shang, Y.; Li, G.; Liu, W.; Ning, Z. Quasi-2D Inorganic CsPbBr3Perovskite for Efficient and Stable Light-Emitting Diodes. *Adv. Funct. Mater.* **2018**, *28*, 1801193.
(24) Wu, C.; Wu, T.; Yang, Y.; McLeod, J. A.; Wang, Y.; Zou, Y.; Zhai, T.; Li, J.; Ban, M.; Song, T.; Gao, X.; Duhm, S.; Sirringhaus, H.; Sun, B. Alternative Type 2D-3D Lead Halide Perovskite with Inorganic Sodium Ions as Spacer for High Performance Light Emitting Diodes. *ACS Nano* **2019**, *13*, 1645−1654.
(25) Ban, M.; Zou, Y.; Rivett, JPH; Yang, Y.; Thomas, TH; Tan, Y.; Song, T.; Gao, X.; Credgington, D.; Deschler, F.; Sirringhaus, H.; Sun, B. Solution-Processed Perovskite Light Emitting Diodes with Efficiency Exceeding 15% through Additive-Controlled Nanostructure Tailoring. *Nat. Commun.* **2018**, *9*, 3892.
(26) Cho, H.; Wolf, C.; Kim, J. S.; Yun, H. J.; Bae, J. S.; Kim, H.; Heo, J.-M.; Ahn, S.; Lee, T.-W. High-Efficiency Solution-Processed Inorganic Metal Halide Perovskite Light-Emitting Diodes. *Adv. Mater.* **2017**, *29*, 1700579.
(27) Lee, S. Y.; Nam, Y. S.; Yu, J. C.; Lee, S.; Jung, E. D.; Kim, S.-H.; Lee, S.; Kim, J.-Y.; Song, M. H. Highly Efficient Flexible Perovskite Light-Emitting Diodes Using the Modified PEDOT:PSS Hole Transport Layer and Polymer-Silver Nanowire Composite Electrode. *ACS Appl. Mater. Interfaces* **2019**, *11*, 39274−39282.
(28) Xie, C.; You, P.; Liu, Z.; Li, L.; Yan, F. Ultrasensitive Broadband Phototransistors Based on Perovskite/Organic-Semiconductor Vertical Heterojunctions. *Light: Sci. Appl.* **2017**, *6*, No. e17023.
(29) Long, H.; Peng, X.; Lu, J.; Lin, K.; Xie, L.; Zhang, B.; Ying, L.; Wei, Z. Exciton-phonon interaction in quasi-two dimensional layered (PEA)2(CsPbBr3)n−1PbBr4 perovskite. *Nanoscale* **2019**, *11*, 21867−21871.
(30) Yuan, S.; Wang, Z. K.; Xiao, L. X.; Zhang, C. F.; Yang, S. Y.; Chen, B. B.; Ge, H. T.; Tian, Q. S.; Jin, Y.; Liao, L. S. Optimization of Low-Dimensional Components of Quasi-2D Perovskite Films for Deep-Blue Light-Emitting Diodes. *Adv. Mater.* **2019**, *31*, 1904319.
(31) Chen, Y.; Sun, Y.; Peng, J.; Tang, J.; Zheng, K.; Liang, Z. 2d Ruddlesden-Popper Perovskites for Optoelectronics. *Adv. Mater.* **2018**, *30*, 1703487.
(32) Yuan, S.; Wang, Z.-K.; Zhuo, M.-P.; Tian, Q.-S.; Jin, Y.; Liao, L.-S. Self-Assembled High Quality CsPbBr3 Quantum Dot Films toward Highly Efficient Light-Emitting Diodes. *ACS Nano* **2018**, *12*, 9541−9548.
(33) Wang, S.; Ma, J.; Li, W.; Wang, J.; Wang, H.; Shen, H.; Li, J.; Wang, J.; Luo, H.; Li, D. Temperature-Dependent Band Gap in Two-Dimensional Perovskites: Thermal Expansion Interaction and Electron-Phonon Interaction. *J. Phys. Chem. Lett.* **2019**, *10*, 2546−2553.
(34) Zhang, Y.; Wang, R.; Li, Y.; Wang, Z.; Hu, S.; Yan, X.; Zhai, Y.; Zhang, C.; Sheng, C. Optical Properties of Two-Dimensional Perovskite Films of (C6H5C2H4NH3)2[PbI4] and (C6H5C2H4NH3)2 (CH3NH3)2[Pb3I10]. *J. Phys. Chem. Lett.* **2019**, *10*, 13−19.
(35) Wei, Q.; Mukaida, M.; Naitoh, Y.; Ishida, T. Morphological Change and Mobility Enhancement in PEDOT:PSS by Adding Co-Solvents. *Adv. Mater.* **2013**, *25*, 2831−2836.
(36) Yu, J.; Wang, N.; Zang, Y.; Jiang, Y. Organic Photovoltaic Cells Based on TPBI as a Cathode Buffer Layer. *Sol. Energy Mater. Sol. Cells* **2011**, *95*, 664−668.
(37) Yuan, M.; Quan, L. N.; Comin, R.; Walters, G.; Sabatini, R.; Voznyy, O.; Hoogland, S.; Zhao, Y.; Beauregard, E. M.; Kanjanaboos, P.; Lu, Z.; Kim, D. H.; Sargent, E. H. Perovskite Energy Funnels for Efficient Light-Emitting Diodes. *Nat. Nanotechnol.* **2016**, *11*, 872−877.

https://dx.doi.org/10.1021/acsami.0c13214
ACS Appl. Mater. Interfaces 2020, 12, 43331−43338